In Situ Study of CO2 and H2O Partitioning Between Na-Montmorillonite and Variably Wet Supercritical Carbon Dioxide.

ARTICLE *in* LANGMUIR · MAY 2014

Impact Factor: 4.46 · DOI: 10.1021/la500682t · Source: PubMed

Langmuir

Article

pubs.acs.org/Langmuir

In Situ Study of CO_2 and H_2O Partitioning between Na–Montmorillonite and Variably Wet Supercritical Carbon Dioxide

John S. Loring,* Eugene S. Ilton, Jeffrey Chen, Christopher J. Thompson, Paul F. Martin, Pascale Bénézeth, Kevin M. Rosso, Andrew R. Felmy, and Herbert T. Schaef

Pacific Northwest National Laboratory, Richland, Washington 99352, United States

Supporting Information

ABSTRACT: Shale formations play fundamental roles in large-scale geologic carbon sequestration (GCS) aimed primarily to mitigate climate change and in smaller-scale GCS targeted mainly for CO_2-enhanced gas recovery operations. Reactive components of shales include expandable clays, such as montmorillonites and mixed-layer illite/smectite clays. In this study, *in situ* X-ray diffraction (XRD) and *in situ* infrared (IR) spectroscopy were used to investigate the swelling/shrinkage and H_2O/CO_2 sorption of Na^+-exchanged montmorillonite, Na-SWy-2, as the clay is exposed to variably hydrated supercritical CO_2 ($scCO_2$) at 50 °C and 90 bar. Measured d_{001} values increased in stepwise fashion and sorbed H_2O concentrations increased continuously with increasing percent H_2O saturation in $scCO_2$, closely following previously reported values measured in air at ambient pressure over a range of relative humidities. IR spectra show H_2O and CO_2 intercalation, and variations in peak shapes and positions suggest multiple sorbed types of H_2O and CO_2 with distinct chemical environments. Based on the absorbance of the asymmetric CO stretching band of the CO_2 associated with the Na-SWy-2, the sorbed CO_2 concentration increases dramatically at sorbed H_2O concentrations from 0 to 4 mmol/g. Sorbed CO_2 then sharply decreases as sorbed H_2O increases from 4 to 10 mmol/g. With even higher sorbed H_2O concentrations as saturation of H_2O in $scCO_2$ was approached, the concentration of sorbed CO_2 decreased asymptotically. Two models, one involving space filling and the other a heterogeneous distribution of integral hydration states, are discussed as possible mechanisms for H_2O and CO_2 intercalations in montmorillonite. The swelling/shrinkage of montmorillonite could affect solid volume, porosity, and permeability of shales. Consequently, the results may aid predictions of shale caprock integrity in large-scale GCS as well as methane transmissivity in enhanced gas recovery operations.

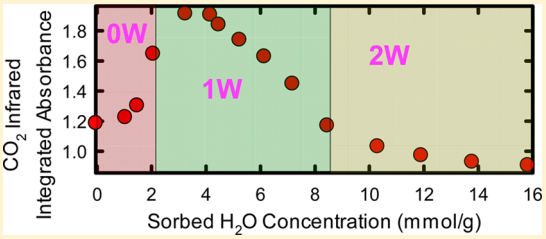

1. INTRODUCTION

Geologic carbon sequestration (GCS) is aimed at slowing the increase of atmospheric carbon dioxide by capturing and storing anthropogenic-sourced CO_2 as a supercritical fluid ($scCO_2$) in a deep geologic reservoir. Shale formations play key functions in GCS, but the geochemistry between shale minerals, CO_2, and water under reservoir temperatures and pressures is not well understood. Large-scale GCS typically depends on shale-dominated caprocks to trap injected $scCO_2$ in high storage capacity sandstones and to prevent its upward migration.[1] Small-scale GCS has been recently suggested to use CO_2 in enhanced gas recovery (EGR) operations, primarily to increase methane production from fractured gas-bearing shale formations and optionally to sequester CO_2 at depth for long-term storage.[2−4] Shale mineralogy varies widely; some shales are carbonate- or silt-rich whereas others are dominated by clays minerals (phyllosilicates), such as illite, chlorite, smectite, and kaolinite.[5] For the most part, clays determine the key physical traits (i.e., permeability, brittleness) and certain chemical properties (i.e., wettability, gas adsorption) of shales.[6,7] Therefore, over a broad scope of GCS operations, it is essential to understand how the clay minerals in shales respond to H_2O-bearing $scCO_2$ fluids to better predict caprock sealing integrity, reservoir storage capacity, and optimal methane recovery conditions.

Montmorillonites are an important class of clays found in shales. These minerals are 2:1 phyllosilicates with ideal stoichiometry $[(Na,Ca)_{0.33}(Al,Mg)_2(Si_4O_{10})(OH)_2{\cdot}nH_2O]$ that can swell and shrink by interlayer uptake (intercalation) and release of H_2O and, under certain conditions, CO_2.[8−13] Swelling of montmorillonites by intercalation of H_2O results in hydration states that are typically referred to as 0W, 1W, or 2W, based on layer-to-layer spacings (d_{001} reflection values) measured by X-ray diffraction (XRD). These designations simplistically refer to 0, 1, or 2 planes of H_2O molecules between the 2:1 layers.[14,15] However, such a description is inadequate for geologic sequestration scenarios where both H_2O and CO_2 could exchange into the interlayer of the clay. Therefore, in this article, the use of 0W, 1W, or 2W does not refer to the actual number of H_2O layers, but instead to the corresponding d_{001} values as if 0, 1, or 2 planes of only H_2O were present.

Received: February 25, 2014
Revised: May 7, 2014
Published: May 8, 2014

   dx.doi.org/10.1021/la500682t | *Langmuir* 2014, 30, 6120−6128

A vast knowledge base of the swelling and shrinkage of montmorillonites at ambient conditions already exists. For example, in the 1990s, Cases and co-workers[16,17] used a multitechnique approach to elucidate the mechanisms of H_2O sorption and to track the distribution of sorbed H_2O over external and interlayer surfaces as a function of relative humidity. In 2005, Ferrage[14] used XRD profile fitting to determine the distribution interlayer hydration states as a function of relative humidity and thus refined interlayer structural parameters.[14] Morodome and Kawamura[18] investigated the effect of temperature, from 50 to 150 °C, on the swelling behavior of montmorillonites. They measured d_{001} values using XRD as a function of relative humidity and observed little impact on the hydration state of Na−montmorillonite with temperature.[18] Johnston and coauthors[19−21] used infrared (IR) spectroscopy to investigate the molecular-level properties of interlayer H_2O as a function of sorbed H_2O concentration. For example, they distinguished H_2O bound directly to the interlayer cation from those occupying cation−void interlayer space and pore space.[19−21]

More recently, research has focused on montmorillonite swelling−shrinkage reactions in $scCO_2$ under conditions relevant to GCS. In 2012, Schaef et al.[10,12] observed by *in situ* XRD that exposure of a sub-1W montmorillonite to dry $scCO_2$ expands the interlayer, which is a response that may increase solid volume and potentially improve well bore and caprock integrity. However, they showed that a 2W clay will dehydrate when exposed to anhydrous $scCO_2$, decreasing solid volume.[10,12] Also in 2012, Giesting et al. showed by *in situ* XRD that montmorillonite can expand by as much as 9%, depending on initial H_2O content of the clay after exposure to pressurized dry $scCO_2$.[8,9] Whereas the expansion of clays exposed to $scCO_2$ provides indirect evidence of CO_2 intercalation, direct evidence was reported by Loring et al. in 2012 by a combination of *in situ* IR and ^{13}C nuclear magnetic resonance (NMR) spectroscopies.[11] Soon after, Rother et al. used *in situ* neutron diffraction measurements to show that exposure of a sub-1W montmorillonite to dry $scCO_2$ produces not only clay expansion but also an increase in the density of the interlayer, combining structural and phase-contrast evidence for intercalation of CO_2.[13] In addition to experimental work, molecular dynamics (MD) simulations explored interlayer structure and spacing changes with CO_2 intercalation at supercritical pressures and temperatures.[22−24] Results show calculated preferred geometric configurations and vibrational spectra of the incorporated CO_2, the influence of intercalated CO_2 on interlayer cation coordination, and d_{001} values as a function of interlayer H_2O and CO_2 concentrations.[22−24]

Whereas CO_2 can diffuse from bulk $scCO_2$ into the interlayer and cause expansion of montmorillonite, this intercalation process was demonstrated only for sub-1W clays after exposure to anhydrous $scCO_2$.[8−12] A comprehensive and fundamental understanding of the role of CO_2 in clay swelling or shrinkage at geologic reservoir conditions requires experimental investigations over the full range of H_2O contents in $scCO_2$, from 0 to 100% saturated. The extent of montmorillonite expansion is likely a complex function of not only interlayer cation type, layer charge, and intercalated H_2O content but also the concentration of CO_2 in the interlayer. Likewise, CO_2 sorption capacity of expandable clays when exposed to $scCO_2$ must depend on the activity of H_2O in the system. To date, there has been no systematic experimental study on CO_2−H_2O partitioning between a clay and variably hydrated $scCO_2$.

Here, a quantitative and molecular-level experimental approach was used to correlate clay expansion and H_2O/CO_2 partitioning between variably wet $scCO_2$ and Na^+-saturated montmorillonite, Na-SWy-2, at GCS relevant conditions (50 °C and 90 bar). Results for the montmorillonite are compared to parallel experiments on pure kaolinite, KGa-1. Kaolinite is a 1:1 phyllosilicate that is typically regarded as nonexpandable, thus serving as a control that lacks an accessible interlayer. The goals were to (1) determine values for the layer spacing of montmorillonite as a function of the percent H_2O saturation in $scCO_2$, which ultimately can be used to predict solid volume changes that affect shale permeability in GCS and related CO_2-EGR applications, and (2) provide a fundamental understanding of montmorillonite swelling−shrinkage at GCS pressures and temperatures. For the latter, sorbed H_2O and CO_2 were characterized at a molecular level in speciation and structure, and trends in sorbed CO_2 concentrations were considered with published models for clay hydration.

2. EXPERIMENTAL SECTION

Naturally occurring montmorillonite from Wyoming (SWy-2) and kaolinite from Georgia (KGa-1) were obtained from the Clay Mineral Repository (Columbia, MO) of the Clay Mineral Society. Clay samples were processed to obtain <2 μm size fractions, and the SWy-2 aliquot was saturated with Na^+, according to previously described methods.[10,12,15] The clays, as processed, have been previously well characterized.[25−31]

Layer-to-layer spacings (d_{001} values) and H_2O concentrations in $scCO_2$ were correlated by coupling an *in situ* pressurized XRD[10,12] with an *in situ* flow-through transmission IR capability,[32,33] as described below. Experiments were conducted at 50 °C and 90 bar. In each run, an aliquot of Na-SWy-2 suspension was pipetted onto a sample post of the high-pressure XRD cell and allowed to air-dry. Then, the XRD cell was mounted in a temperature-controlled apparatus designed to circulate a stream of $scCO_2$ past the clay sample in a closed flow loop. The system includes stainless steel tubing, switching valves, pressure vessels, an HPLC pump, and an in-line transmission cell mounted within an IR spectrometer (see Figure S1, Supporting Information).[32,33] After pressurizing the apparatus with anhydrous $scCO_2$, the fluid was circulated by the HPLC pump, and a background IR spectrum was measured. Next, water was injected into the flow loop, and the concentration of H_2O in the $scCO_2$ stream was monitored by the IR absorbance of the HOH bending mode (1608 cm^{-1}). After 3−15 h of equilibration, the isolated XRD cell was transferred to the X-ray diffractometer. The pressurized cell was maintained at 50 °C during the transfer and subsequent XRD data acquisition. Percent H_2O saturation was calculated from the ratio of the IR absorbance of the HOH bending mode to that determined from an independent measurement of $scCO_2$ completely saturated with H_2O. Diffraction patterns, processed with JADE software (MDI, Version 9.5), were collected to monitor shifts and overall peak shapes in the d_{001} reflection.

In situ high-pressure titrations with IR detection were performed at 50 °C and 90 bar using a fully automated $scCO_2$ generation and delivery apparatus coupled to a high-pressure IR cell with transmission and attenuated total reflection (ATR) IR optics. The cell is similar to that of Schneider et al.[34] and consists of a jacketed 53 mL stainless-steel vessel (SITEC Sieber Engineering AG, Zurich, Switzerland) that is temperature-controlled by a circulating water bath. The transmission IR optics consist of cylindrical ZnSe windows and a path length of ~1 mm. The internal reflection element (IRE) of the ATR IR optics is a single-reflection 45° prism made of ZnSe (Harrick Scientific). Further details of the high-pressure IR titration system and the method for performing titrations of clay samples are reported elsewhere[35] and briefly described in the Supporting Information.

dx.doi.org/10.1021/la500682t | *Langmuir* 2014, 30, 6120−6128

3. RESULTS

Figure 1 is a summary plot of XRD data for Na-SWy-2 and transmission IR results (see below) from titrations of Na-SWy-2 and KGa-1. The XRD data show layer spacings (d_{001}/Å) plotted versus concentration of H_2O in $scCO_2$, as a percentage of the concentration to saturate $scCO_2$. The percent H_2O saturation values were determined from IR measurements obtained as each sample was equilibrated in the XRD cell with wet $scCO_2$ (see Experimental Section). The Na-SWy-2 hydration state was based on layer spacings of 9.6−10.1 Å at 0W, 12.3−12.7 Å at 1W, and 15.0−15.8 Å at 2W.[14,36] Figure 1 shows that the hydration states of Na-SWy-2 display common stepwise behavior with percent H_2O saturation: 0W from about 0 to 20% saturation, 1W from about 20% to 70%, and 2W from about 70% to 90%.

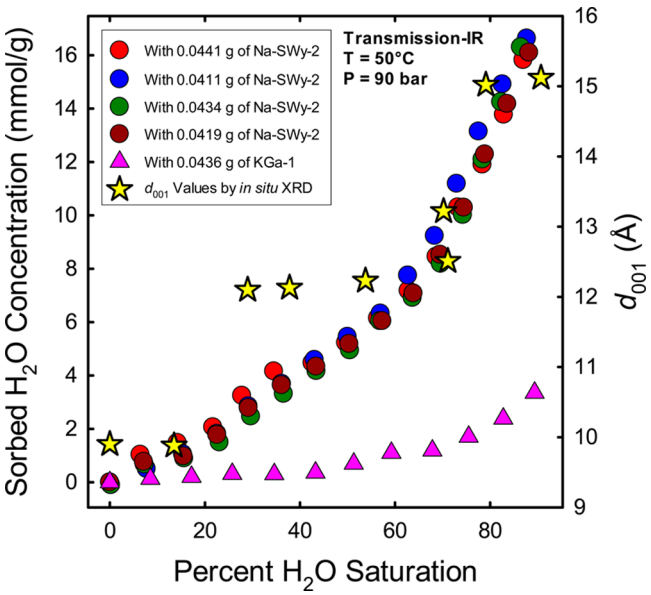

Figure 1. Sorbed H_2O concentrations as a function of the percent H_2O saturation in the $scCO_2$ for titrations of Na-SWy-2 and KGa-1 with water at 50 °C and 90 bar. The precision in the sorbed H_2O concentrations is estimated ±1.0 mmol/g. Also shown are the d_{001} values of Na-SWy-2 from XRD measurements at the same temperature and pressure conditions.

Three IR spectroscopic titrations of $scCO_2$ with H_2O were performed at 50 °C and 90 bar in the absence of clay to obtain calibration curves to quantify dissolved H_2O concentrations and to determine the solubility of H_2O. In Figure S2 (see Supporting Information), the transmission IR integrated absorbance of the HOH bending mode of H_2O dissolved in $scCO_2$ is reported as a function of the total H_2O concentration. As concentration increases, the integrated absorbance rises linearly until a plateau is reached, indicating that the fluid is saturated with H_2O. The saturation point is the H_2O concentration at the intersection of the straight lines that are fit through the data points in the linear and plateau regions. The measured H_2O solubility based on three independent titrations was 36 ± 1 mM. This is in close agreement with a previously reported value of 33 ± 3 mM at the same temperature and pressure that was determined by using near-IR spectroscopy.[37] However, our measured value is higher than that predicted for similar conditions by the mutual CO_2−H_2O solubility model of Spycher et al. (23 mM)[38] as well as the experimental values cited therein.

IR spectroscopic titrations of Na-SWy-2 and KGa-1 with H_2O in $scCO_2$ were performed to (1) quantify the partitioning of H_2O and CO_2 between the supercritical fluid and the clay and (2) obtain molecular-level information about sorbed H_2O and CO_2. One titration was performed for KGa-1, whereas four were performed with Na-SWy-2. Figure S2 (see Supporting Information) shows the integrated absorbance by transmission IR under the HOH bending mode of H_2O dissolved in the $scCO_2$ as a function of the total H_2O concentration. The difference between the integrated absorbances where clay is present and absent (i.e., the H_2O calibration curves) can be used to calculate the concentration of H_2O sorbed by the clays. Furthermore, the concentration of H_2O remaining in the supercritical fluid and the concentration of H_2O needed to saturate the $scCO_2$ can be used to determine the percentage of H_2O saturation for each water addition during the titrations. In Figure 1, the concentration of sorbed H_2O in millimoles per

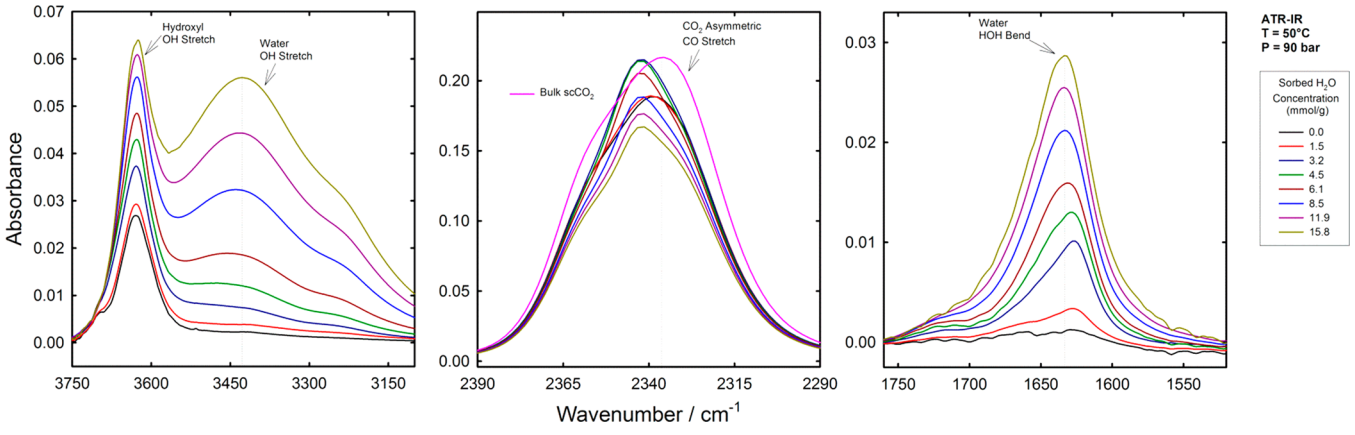

Figure 2. ATR IR spectra as a function of sorbed H_2O concentration from a titration of 0.0441 g of Na-SWy-2 with water at 50 °C and 90 bar. Spectra have been baseline corrected by subtracting the lines fit through the average absorbances between 2625−2725 cm^{-1} and 4000−4100 cm^{-1} for the OH stretching region (left panel), 2140−2160 cm^{-1} and 2560−2580 cm^{-1} for the CO_2 asymmetric CO stretching region (center panel), and 1400−1440 cm^{-1} and 1800−1880 cm^{-1} for the HOH bending region (right panel). ATR IR spectra are only shown for every second addition of the titration (i.e., every other data point in Figure 1) for clarity. In the middle panel, a spectrum of bulk $scCO_2$ in the absence of any clay is shown for comparison.

dx.doi.org/10.1021/la500682t | Langmuir 2014, 30, 6120−6128

gram of clay (mmol/g) is shown versus percent H_2O saturation for all four Na-SWy-2 titrations and the KGa-1 titration.

The ATR IR spectra from titrations of 0.0441 g of Na-SWy-2 and 0.0436 g of KGa-1 are reported in Figure 2 and Figure S3 (see Supporting Information), respectively. Changes as a function of sorbed H_2O concentration are observed in the OH stretching and HOH bending mode regions of H_2O and in the asymmetric CO stretching band region of CO_2. Only small perturbations are apparent in the SiO stretching bands of the montmorillonite clay as it hydrates, and essentially no changes are observed in these bands for kaolinite. The OCO bending mode of CO_2 at 664 cm^{-1} is not given because the signal-to-noise is poor in this region—the ZnSe IRE absorbs most of the IR radiation below 700 cm^{-1}. The reaction of CO_2 with the interlayer metal cation of montmorillonite or with metal cations released from clay dissolution could lead to the formation of a metal carbonate, which would be indicated by the growth of CO stretching bands of carbonate in the wavenumber range between about 1200 and 1600 cm^{-1}. No changes in this region are observed, and thus there is no evidence of a carbonation reaction, which is in contrast to the *ex situ* findings of Hur et al. and Romanov.[39,40]

The left panel of Figure 2 and Figure S3 (see Supporting Information) shows the OH stretching bands of hydroxyls in the clay layers and H_2O sorbed in and on the clay, and the right panel shows the HOH bending mode of the clay-associated H_2O. As total H_2O concentration increases in $scCO_2$, H_2O sorption increases, as indicated by an increase in the absorbance of the OH stretching and HOH bending modes. These changes are consistent with the increase in sorbed H_2O determined from the transmission measurements (see Figure 1). For Na-SWy-2 (Figure 2), subtle changes in the band shapes and peak positions of the OH stretching and HOH bending modes indicate that more than one type of molecular environment for the sorbed H_2O occurs. In contrast, the spectra from the titration of KGa-1 (Figure S3, see Supporting Information) show much lower intensity in the OH stretching and HOH bending modes, and band perturbations with increasing total H_2O concentrations are less apparent. To further investigate the changes with sorbed H_2O concentration in the titration data for Na-SWy-2, a principal component analysis on the spectral data set for Na-SWy-2 (0 to 15.8 mmol/g and from 1500 to 1800 cm^{-1} and 3100 to 3500 cm^{-1}) was performed. The results are reported in Supporting Information (Figure S5). Based on systematic patterns in the first four eigenvectors, the rank of the data matrix is four, indicating at least four spectroscopically distinct sources of variance.

The center panel of Figure 2 and Figure S3 (see Supporting Information) shows the ATR IR spectra from clay titrations in the asymmetric CO stretching mode region of CO_2. For comparison, the spectrum of bulk $scCO_2$ is shown from an independent measurement in the absence of clay or H_2O. Because the infrared radiation penetrates beyond the overlayer, the bulk $scCO_2$ contributes to the IR spectra. Differences between the asymmetric CO stretching band of bulk $scCO_2$ and the band in the spectra from the KGa-1 titration are small. In contrast, the differences between bulk $scCO_2$ and the spectra from the Na-SWy-2 titration are striking, providing direct evidence of CO_2 intercalation into the clay interlayer.[11]

The asymmetric CO stretching band of the CO_2 molecules associated with the clay can be isolated by subtracting the spectrum of bulk $scCO_2$ from the clay titration spectrum. Difference spectra for one titration of Na-SWy-2 and the KGa-1 titration are in Figure 3 and Figure S4 (see Supporting Information), respectively. The subtrahend factor for the difference spectra was estimated to be inversely correlated to the sorbed H_2O concentration determined from transmission IR (see Figure 1). Details regarding the determination of this subtrahend factor are reported in the Supporting Information.

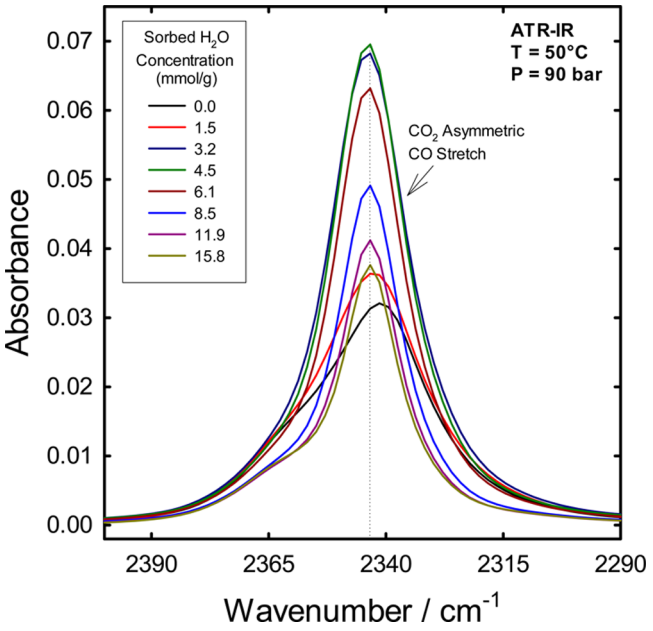

Figure 3. ATR IR spectra as a function of sorbed H_2O concentration showing the asymmetric CO stretching band of the CO_2 molecules that are associated with Na-SWy-2. These spectra are those shown in the center panels of Figure 2 from a titration of 0.0441 g of Na-SWy-2 with water at 50 °C and 90 bar, but they have processed as described in the text so that the spectral contributions of bulk $scCO_2$ have been removed.

Two features in the spectra of the CO_2 molecules associated with Na-SWy-2 (Figure 3) in the asymmetric CO stretching band region are a peak at ~2343 cm^{-1} and a minor shoulder at ~2356 cm^{-1}. Whereas the intensity of the shoulder remains nearly the same with increasing H_2O concentration, the intensity of the peak at 2343 cm^{-1} increases significantly as the sorbed H_2O concentration increases from 0.0 to 4.5 mmol/g, but then decreases steadily in absorbance thereafter. A principal component analysis to investigate changes in the CO stretching band with sorbed H_2O concentration was performed at H_2O concentrations from 0 to 15.8 mmol/g and in the region between 2200 and 2500 cm^{-1} (Supporting Information, Figure S6). The rank of the data matrix is four, indicating four spectroscopically distinct sources of variance.

Similar to the Na-SWy-2 data, the KGa-1 spectra (Figure S4, see Supporting Information) show a dominant peak at 2343 cm^{-1} and a shoulder at ~2356 cm^{-1}. As the sorbed H_2O concentration increases from 0.0 to 2.4 mmol/g, the intensity of the peak at 2343 cm^{-1} increases slightly, but the absorbance due to the shoulder remains nearly unchanged. In comparison to Na-SWy-2 (Figure 3), the overall variation in the asymmetric CO stretching band of the CO_2 molecules associated with KGa-1 (Figure S4, see Supporting Information) is relatively small.

dx.doi.org/10.1021/la500682t | *Langmuir* 2014, 30, 6120−6128

4. DISCUSSION

The layer spacings for Na-SWy-2 as a function of percent H_2O saturation in $scCO_2$ (Figure 1) closely match spacings measured on sodium saturated montmorillonites at 50 °C and ambient pressure as a function of relative humidity.[18] The observed stepwise expansion is referred to as "crystalline swelling", where layer spacings have a number of stable values that discontinuously increase with increasing total H_2O activity. These values result from the incorporation of discrete and organized planes of H_2O, which depend on complex and related factors such as interlayer cation type and layer charge density.[41] Likewise, the sorbed H_2O concentrations (Figure 1) are similar to those reported for this clay at 25 °C and ambient pressure.[16,20] For example, the maximum sorbed H_2O concentration at 90% saturation is ~16 mmol/g, which is similar to that reported by Cases et al.[16] and Xu et al.[21] for 90% relative humidity in air. The ranges of sorbed H_2O concentrations at XRD-determined hydration states are also consistent with data at ambient conditions.[14,16] In $scCO_2$ at 50 °C and 90 bar, concentrations of about 0−2 mmol/g of sorbed H_2O are present for the 0W state (9.6−10.1 Å), 3−8 mmol/g for the 1W state (12.3−12.7 Å), and 8−16 mmol/g for the 2W state (15.0−15.8 Å). These are comparable to about 0−2, 2−9, and 9−16 mmol/g for the 0W, 1W, and 2W states, respectively, in humid air at 25 °C and 1 bar.[14,16,20,21] That the clay behaves similarly in $scCO_2$ and in air at ambient conditions might seem unexpected, given that the absolute concentration of H_2O in saturated $scCO_2$ is 36.1 mM in $scCO_2$ at 50 °C and 90 bar versus only 4.6 mM in saturated air at 50 °C and 1 bar.[42] However, despite the large difference in absolute water concentrations at these two conditions, the key thermodynamic parameter controlling clay expansion is the *percentage* of the H_2O saturation concentration.

Whereas exposure of sub-1W montmorillonites to dry $scCO_2$ causes interlayer expansion up to 9% by CO_2 intercalation,[8−12] the similarity of our structural and H_2O sorption data with previous work at ambient pressure in air and at various temperatures[18] indicates that a CO_2 pressure of 90 bar does not significantly affect interlayer expansion or H_2O sorption at above the 1W hydration state. This result was unexpected because neutron diffraction and modeling studies have suggested that increasing hydrostatic pressure at fixed temperature increases the affinity of H_2O in the interlayer of expandable clays.[43−45] A previous study on the interaction of Na-STx-1 (Na^+-exchanged montmorillonite from Texas) with variably wet $scCO_2$ at 50 °C and 90 bar[10] indicated that a 3W hydration state was achieved well below 100% H_2O saturation. However, the percent H_2O saturation in $scCO_2$ was not directly measured but instead estimated using a number of assumptions.

Although the d_{001} values increase in stepwise fashion with increasing percent H_2O saturation in $scCO_2$, sorbed H_2O increases smoothly (Figure 1), as previously noted at ambient pressures.[14,16,19,20] This is partly explained in that total sorbed H_2O is linear combination of sorbed H_2O in the interlayer, on external clay surfaces, and in pore space. Because kaolinite has no accessible interlayer region for H_2O, a comparison of the sorbed H_2O concentrations (Figure 1) between the KGa-1 and Na-SWy-2 titrations approximates externally sorbed and pore space H_2O contributions to the montmorillonite data.[46] A first-order comparison between KGa-1 and Na-SWy-2 is possible because these minerals have external surfaces areas that are within about a factor of 2.[46−48] Consistent with estimates by Ferrage et al.,[14,49] the kaolinite results suggest that the concentration of H_2O on external sites and in pores only becomes significant between about 70 and 90% H_2O saturation in $scCO_2$. However, half of the external surfaces of kaolinite are aluminum hydroxide gibbsite-like layers that are more hydrophilic than the exclusively siloxane basal planes of montmorillonite.[50] Thus, the kaolinite data may overestimate the contribution of external sites and pores to the total sorbed H_2O concentration on montmorillonite.

Consequently, below 70% H_2O saturation, H_2O sorption in montmorillonite is likely dominated by uptake in the interlayer. Two models reconcile the apparent contradiction between the continuous increase in sorbed interlayer H_2O but discontinuous increase in d_{001} values. First, in a space-filling model adapted from Cases et al.,[16,51,52] montmorillonite is assumed to be homogeneous with respect to hydration state at any given H_2O activity. With increasing H_2O activity, a threshold is reached where a limited amount of H_2O hydrates the interlayer cations and expands the clay from 0W to a d_{001} value associated with the 1W state; however, there is space available that allows further hydration without additional interlayer expansion. Once this void space is fully occupied, another threshold is reached where a minimum increase in H_2O expands the clay from 1W to a d_{001} value characteristic of the 2W state; the process repeats creating voids and the possibility for further hydration where a plateau in the d_{001} value is maintained.

Second, in a hydration−heterogeneity model, a distribution of individual interlayers with integral hydrations states (i.e., d_{001} values characteristic of 0W, 1W, or 2W) exists at a given percent H_2O saturation.[14,16,48,50] As the percent H_2O saturation is increased starting from anhydrous, the montmorillonite shifts from predominantly 0W, to a mixture of 0W + 1W, to predominantly ~1W, to a mixture of 1W + 2W, to predominantly ~2W. The XRD data described here show d_{001} peak-width changes and shoulders as a function of total H_2O and apparently support this model. However, Figure 1 shows a plot of only maximum peak-height positions for the d_{001} reflections because higher order reflections are too weak to derive component hydration states.

In summary, the space-filling and hydration−heterogeneity models attempt to reconcile the continuous sorption of H_2O with the stepwise increase in d_{001} values in two different ways. As conceptual models, they do not fully explain the partitioning of CO_2 and H_2O between $scCO_2$ and montmorillonite over the full range of H_2O activity, as discussed below.

Principal component analysis of the ATR IR spectra from the titration of Na-SWy-2 for the OH stretching and HOH bending modes of sorbed H_2O indicated at least four spectroscopically distinct types of H_2O (Figure S5). Johnston et al. and Xu et al.[20,21] discussed peak shifts and adsorption coefficient changes of the OH stretching and HOH bending modes as a function of sorbed H_2O concentration. Some of these spectral contributions are related to H_2O that are bound inner-spherically to the interlayer cation at low sorbed H_2O concentrations and to waters with a hydrogen-bonding network approaching that of bulk water at high sorbed H_2O concentrations.[20,21] The spectral characteristics of these two extremes of H_2O environments are the likely cause of the majority of the variance in the ATR IR spectra in the OH stretching and HOH bending mode regions. In addition, some variance is probably related to other coordination environments and interactions, including the second hydration shell of Na^+, external sorption sites, and interactions with cosorbed CO_2.

dx.doi.org/10.1021/la500682t | Langmuir 2014, 30, 6120−6128

The dominant spectral feature of CO_2 associated with Na-SWy-2 and KGa-1 (Figure 3 and Figure S4 in Supporting Information, respectively) is a peak at ~2343 cm^{-1} with a minor shoulder near ~2356 cm^{-1}. In an *ex situ* study, Romanov[40] also reported a peak at ~2343 cm^{-1} of similar width for CO_2 associated with SWy-2 after depressurization from an experiment where the clay was exposed to $scCO_2$. The position and shape of the band at ~2343 cm^{-1} strongly resemble the asymmetric CO stretching band of CO_2 dissolved in bulk water (Figure S7, Supporting Information). Thus, this peak is probably due to CO_2 associated with H_2O or to CO_2 that has similar chemical properties as CO_2 dissolved in water. This interpretation is consistent with the conclusions drawn from density functional theory (DFT)-MD calculations of the vibrational spectra of CO_2 in water clusters and CO_2 in the hydrated montmorillonite interlayer by Myshakin et al.[24] The shoulder near ~2356 cm^{-1} is related to a "mirage-like" optical effect that is caused by a difference in electric field intensity of the infrared radiation between the two-phase system consisting of a ZnSe IRE and bulk $scCO_2$ and the three-phase system consisting of a clay overlayer between the ZnSe IRE and bulk $scCO_2$. More details on this mirage-like optical effect are reported in the Supporting Information.

Principal component analysis of the spectra of CO_2 associated with Na-SWy-2 (Figure 3) in the asymmetric CO stretching band region indicated at least four spectroscopically distinct sources of variance. As discussed above, the shoulder at ~2356 cm^{-1} is probably a physical−optical effect. Because of a small variation in this optical phenomenon with a change in the refractive index of the clay as the clay hydrates, the shoulder may account for two of the principal components. In contrast, the peak at 2343 cm^{-1} is related to sorbed CO_2 in a variably hydrated environment, and the peak shape narrows and shifts by less than 2 cm^{-1} with increasing sorbed H_2O concentration. The variation in this band probably accounts for the other two sources of variance, indicating that there are at least two types of CO_2 molecules that are distinguished by their proximity to surrounding H_2O, cations, and clay surfaces.

Figure 4 shows the integrated absorbance of the asymmetric CO stretching band of the CO_2 molecules associated with Na-SWy-2 (see Figure 3) as a function of sorbed H_2O concentration. Assuming that the absorption coefficients of the different types of sorbed CO_2 molecules are similar, then the area under this band is proportional to the sorbed CO_2 concentration. Unfortunately, the adsorption coefficient is not known at this time, and the trend is only semiquantitative. Together with the d_{001} values from the XRD measurements, the results show a significant increase in the sorbed CO_2 as the clay expands from a 0W to a 1W state, with a maximum sorbed CO_2 concentration at 4 mmol/g of sorbed H_2O. The concentration of CO_2 then decreases sharply from ~4 to 10 mmol/g of sorbed H_2O, followed by a slower decrease from 10 to 15.8 mmol/g. This behavior is consistent with the MD study of Botan et al.[22] where montmorillonite equilibrated with hydrated $scCO_2$ showed a decrease in interlayer CO_2 from a 1W to 2W hydration state.

Two models of this competitive sorption of H_2O and CO_2 follow from our earlier discussion of the space-filling[16,51,52] and heterogeneous-hydration state models.[14,16,49,51] Considering the latter, at a given temperature and pressure, there is a fixed concentration of CO_2 in the interlayer for a given hydration state, such that the variation in sorbed CO_2 concentration reflects differing linear combinations of 0W, 1W, and 2W hydration states (Figure 4). In previous studies,[10,12,13] the interaction of a sub-1W clay sample with dry $scCO_2$ expanded the interlayer but only yielded a d_{001} value consistent with a 1W clay and never a 2W clay. In fact, Rother et al. provided evidence for a fixed CO_2/H_2O ratio in a 1W montmorillonite equilibrated with $scCO_2$ over a broad range of temperature and pressure.[13] This result places an upper limit on the concentration of interlayer CO_2 under the experimental conditions described here.

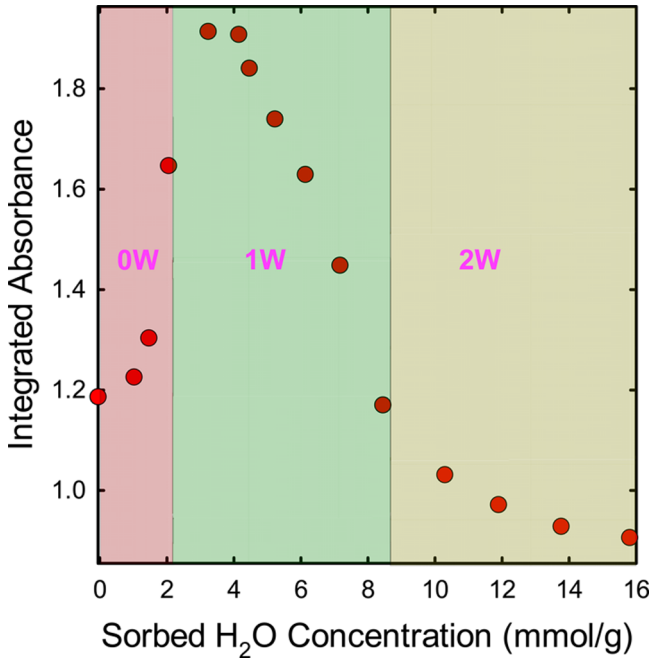

Figure 4. Integrated absorbance of the asymmetric CO stretching band of the CO_2 molecules that are associated with the Na-SWy-2 as a function of sorbed H_2O concentration from a titration of 0.0441 g of Na-SWy-2 with water at 50 °C and 90 bar. The precision in the integrated absorbances values is estimated to be ±0.1.

Alternatively, in the space-filling model, there is an initial influx of CO_2 into the interlayer that correlates with interlayer discrete expansion from a 0W to 1W state. Thus, H_2O props the interlayer open, and CO_2 enters to fill void space. The maximum CO_2 concentration coincides with 4 mmol/g sorbed H_2O. However, as sorbed H_2O concentrations increase from 4 to 8 mmol/g, incorporated CO_2 appears outcompeted by further incoming H_2O for sorption sites (or space) whereas the clay remains in the 1W hydration state (i.e., the d_{001} value is constant as H_2O displaces interlayer CO_2). By analogy, sorbed CO_2 would be expected to increase after the transition from 1W to 2W; however, the data show that sorbed CO_2 continues to decrease, albeit at a slower rate upon transition to the 2W state. Consequently, the space-filling model does not provide a comprehensive mechanism for CO_2 intercalation over the full range of clay hydration states. Further, MD simulations do not support the space-filling model.[24]

Although the space-filling model cannot be completely ruled out, the heterogeneous-hydration state model provides a phenomenological mechanism for the observed partitioning of CO_2 between the clay and $scCO_2$ over the range of H_2O activities studied. Further, it presumes an underlying thermodynamic constraint based on the hydration state of the interlayer that finds support from Rother et al., as discussed above.[13] In addition, recent MD and DFT-based MD

dx.doi.org/10.1021/la500682t | *Langmuir* 2014, 30, 6120−6128

simulations by Myschakin et al.[24] provide molecular-level information on the effect of H_2O concentration on the bonding environment of intercalated CO_2. The calculations show that at relatively low sorbed H_2O concentrations CO_2 interacts with interlayer cations and participates in weak bonds with H_2O. At higher hydration levels, the additional H_2O displaces CO_2 from the inner solvation sphere of the cations and enhances the hydrogen-bonding network.[24] These calculated results are in accord with experimental data reported here and the heterogeneous-hydration state model; intercalated CO_2 may be more stable at low sorbed H_2O concentrations but less stable at higher H_2O concentrations, leading to diffusion of CO_2 back into bulk $scCO_2$. Note, however, that there is no clear evidence in the spectra in Figure 3 that the CO_2 interacts strongly with the interlayer Na^+ at the lowest water concentrations, based on a comparison to calculated results for the spectra of interlayer CO_2 at low H_2O:CO_2 ratios by Myschakin et al.[24]

Above ~8 mmol/g of sorbed H_2O, the sorbed CO_2 concentration decreases asymptotically (see Figure 4). At 15.8 mmol/g sorbed H_2O, the IR spectra indicate that CO_2/H_2O band intensity ratios are similar for Na-SWy-2 and bulk water (Figure S7, Supporting Information), consistent with the solubility of CO_2 in the sorbed H_2O approaching its solubility in bulk water as the system saturates with H_2O in the bulk $scCO_2$ phase.

5. CONCLUSIONS

The partitioning of H_2O and CO_2 into a Na-saturated montmorillonite (Na-SWy-2) has been characterized and linked to the structural layer spacings of the clay as a function of percent H_2O saturation in $scCO_2$ at 50 °C and 90 bar. This unique data set was gathered using novel *in situ* XRD, *in situ* transmission IR, and *in situ* ATR-IR instrumentation. The IR spectra detected only CO_2 and H_2O sorption, and there is no evidence of a carbonation reaction suggested previously.[31,32] The uptake of CO_2 is a complicated function of H_2O activity and was discussed in the context of space-filling and heterogeneous-hydration state models, with the latter being the most comprehensive. Strong limits have been established on the sorbed CO_2 concentration on Na-saturated montmorillonite (Na-SWy-2). In future work, we plan to quantify the sorbed CO_2 concentrations as a function of percent H_2O saturation by obtaining the appropriate absorption coefficients to relate ATR IR absorbance to concentration.

In large GCS operations, injected $scCO_2$ will be contained by a caprock system primarily consisting of shales. Likewise, in the context of CO_2-EGR operations, depleted shale gas reservoirs could yield additional methane while utilizing CO_2, with the added benefit of long-term CO_2 storage. Expandable clays are an important reactive component of many shales, and the present study provides fundamental insights into mechanisms controlling their swelling and shrinkage during exposure to variably wet $scCO_2$ fluids. As demonstrated by our research, H_2O and CO_2 can penetrate the interlayer of montmorillonites at reservoir temperatures and pressures, producing measurable sorbed concentrations and attendant solid volume changes. These measurements are important for developing quantitative reservoir injection strategies that will maintain or enhance shale caprock integrity and maximize shale-gas recovery.

■ ASSOCIATED CONTENT

Supporting Information

(1) A brief description of the method for performing high-pressure IR titrations, (2) further discussions of the effective path length of the infrared radiation, the subtrahend factor of bulk $scCO_2$ spectral subtraction, and the mirage-like optical effect causing the shoulder in the asymmetric CO stretching bands of the CO_2 molecules associated with the clays, (3) a figure showing a schematic of the apparatus used to measure concentrations of dissolved H_2O in $scCO_2$ for the XRD measurements, (4) raw data from transmission IR measurements, (5) ATR IR data for kaolinite, (6) results from chemometrics analyses, and (7) a plot similar to Figure 4 but showing absorbance versus percent H_2O saturation. This material is available free of charge via the Internet at http://pubs.acs.org.

■ AUTHOR INFORMATION

Corresponding Author

*Ph (509) 371-6743; fax (509) 371-6354; e-mail john.loring@pnnl.gov (J.S.L.).

Notes

The authors declare no competing financial interest.

■ ACKNOWLEDGMENTS

We appreciate expert discussions with James E. Amonette as well as useful comments by four particularly insightful reviewers. This work was supported by the U.S. Department of Energy (DOE), Office of Fossil Energy, and by the Geosciences Research Program in the U.S. Department of Energy, Office of Basic Energy Sciences, Division of Chemical Sciences, Geosciences & Biosciences. Development of the instrumentation for this research was funded through Pacific Northwest National Laboratory's Carbon Sequestration Initiative, which was part of a Laboratory Directed Research and Development Program. Several of the experiments were performed using EMSL, the Environmental Molecular Sciences Laboratory, a national scientific user facility sponsored by the DOE's Office of Biological and Environmental Research, and located at PNNL. PNNL is operated for DOE by Battelle Memorial Institute under Contract DE-AC06-76RLO-1830.

■ REFERENCES

(1) Shukla, R.; Ranjith, P.; Haque, A.; Choi, X. A review of studies on CO_2 sequestration and caprock integrity. *Fuel* **2010**, *89*, 2651−2664.

(2) Kang, S. M.; Fathi, E.; Ambrose, R. J.; Akkutlu, I. Y.; Sigal, R. F. Carbon dioxide storage capacity of organic-rich shales. *SPE J.* **2011**, *16*, 842−855.

(3) Busch, A.; Alles, S.; Gensterblum, Y.; Prinz, D.; Dewhurst, D. N.; Raven, M. D.; Stanjek, H.; Krooss, B. M. Carbon dioxide storage potential of shales. *Int. J. Greenhouse Gas Control* **2008**, *2*, 297−308.

(4) Elliot, T. R.; Celia, M. A. Potential restrictions for CO_2 sequestration sites due to shale and tight gas production. *Environ. Sci. Technol.* **2012**, *46*, 4223−4227.

(5) Josh, M.; Esteban, L.; Delle Piane, C.; Sarout, J.; Dewhurst, D. N.; Clennell, M. B. Laboratory characterisation of shale properties. *J. Pet. Sci. Eng.* **2012**, *88*−*89*, 107−124.

(6) Jiang, S. In *Clay Minerals in Nature - Their Characterization, Modification and Application*; Valaškova, M., Martynkova, G. S., Eds.; InTech: Rijeka, Croatia, 2012; p 312.

(7) Gasparik, M.; Bertier, P.; Gensterblum, Y.; Ghanizadeh, A.; Krooss, B. M.; Littke, R. Geological controls on the methane storage capacity in organic-rich shales. *Int. J. Coal Geol.*, in press.

(8) Giesting, P.; Guggenheim, S.; Koster van Groos, A. F.; Busch, A. Interaction of carbon dioxide with Na-exchanged montmorillonite at pressures to 640 bars: Implications for CO_2 sequestration. *Int. J. Greenhouse Gas Control* **2012**, *8*, 73−81.
(9) Giesting, P.; Guggenheim, S.; Koster van Groos, A. F.; Busch, A. X-ray diffraction study of K- and Ca-exchanged montmorillonites in CO_2 atmospheres. *Environ. Sci. Technol.* **2012**, *46*, 5623−5630.
(10) Ilton, E. S.; Schaef, H. T.; Qafoku, O.; Rosso, K. M.; Felmy, A. R. In situ X-ray diffraction study of Na^+ saturated montmorillonite exposed to variably wet super critical CO_2. *Environ. Sci. Technol.* **2012**, *46*, 4241−4248.
(11) Loring, J. S.; Schaef, H. T.; Turcu, R. V.; Thompson, C. J.; Miller, Q. R.; Martin, P. F.; Hu, J.; Hoyt, D. W.; Qafoku, O.; Ilton, E. S.; Felmy, A. R.; Rosso, K. M. In situ molecular spectroscopic evidence for CO_2 intercalation into montmorillonite in supercritical carbon dioxide. *Langmuir* **2012**, *28*, 7125−7128.
(12) Schaef, H. T.; Ilton, E. S.; Qafoku, O.; Martin, P. F.; Felmy, A. R.; Rosso, K. M. In situ XRD study of Ca^{2+} saturated montmorillonite (STX-1) exposed to anhydrous and wet supercritical carbon dioxide. *Int. J. Greenhouse Gas Control* **2012**, *6*, 220−229.
(13) Rother, G.; Ilton, E. S.; Wallacher, D.; Haubeta, T.; Schaef, H. T.; Qafoku, O.; Rosso, K. M.; Felmy, A. R.; Krukowski, E. G.; Stack, A. G.; Grimm, N.; Bodnar, R. J. CO_2 sorption to subsingle hydration layer montmorillonite clay studied by excess sorption and neutron diffraction measurements. *Environ. Sci. Technol.* **2013**, *47*, 205−211.
(14) Ferrage, E.; Lanson, B.; Sakharov, B. A.; Drits, V. A. Investigation of smectite hydration properties by modeling experimental X-ray diffraction patterns: Part I. Montmorillonite hydration properties. *Am. Mineral.* **2005**, *90*, 1358−1374.
(15) Moore, D. M.; Reynolds, R. C. *X-Ray Diffraction and the Identification and Analysis of Clay Minerals*; Oxford University Press: New York, 1989.
(16) Cases, J. M.; Berend, I.; Besson, G.; Francois, M.; Uriot, J. P.; Thomas, F.; Poirier, J. E. Mechanism of adsorption and desorption of water-vapor by homoionic montmorilonite 1. The sodium-exchanged form. *Langmuir* **1992**, *8*, 2730−2739.
(17) Berend, I.; Cases, J. M.; Francois, M.; Uriot, J. P.; Michot, L.; Masion, A.; Thomas, F. Mechanism of adsorption and desorption of water-vapor by homoionic montmorillonites 2. The Li^+, Na^+, K^+, Rb^+ and Cs^+-exchanged forms. *Clays Clay Miner.* **1995**, *43*, 324−336.
(18) Morodome, S.; Kawamura, K. Swelling behavior of Na- and Ca-montmorillonite up to 150°C by *in situ* X-ray diffraction experiments. *Clays Clay Miner.* **2009**, *57*, 150−160.
(19) Johnston, C. T.; Premachandra, G. S. Polarized ATR-FTIR study of smectite in aqueous suspension. *Langmuir* **2001**, *17*, 3712−3718.
(20) Johnston, C. T.; Sposito, G.; Erickson, C. Vibrational probe studies of water interactions with montmorillonite. *Clays Clay Miner.* **1992**, *40*, 722−730.
(21) Xu, W. Z.; Johnston, C. T.; Parker, P.; Agnew, S. F. Infrared study of water sorption on Na-, Li-, Ca-, and Mg-exchanged (SWy-1 and SAz-1) montmorillonite. *Clays Clay Miner.* **2000**, *48*, 120−131.
(22) Botan, A.; Rotenberg, B.; Marry, V.; Turq, P.; Noetinger, B. Carbon dioxide in montmorillonite clay hydrates: thermodynamics, structure, and transport from molecular simulation. *J. Phys. Chem. C* **2010**, *114*, 14962−14969.
(23) Cygan, R. T.; Romanov, V. N.; Myshakin, E. M. Molecular simulation of carbon dioxide capture by montmorillonite using an accurate and flexible force field. *J. Phys. Chem. C* **2012**, *116*, 13079−13091.
(24) Myshakin, E. M.; Saidi, W. A.; Romanov, V. N.; Cygan, R. T.; Jordan, K. D. Molecular dynamics simulations of carbon dioxide intercalation in hydrated Na-montmorillonite. *J. Phys. Chem. C* **2013**, *117*, 11028−11039.
(25) Chipera, S. J.; Bish, D. L. Baseline studies of The Clay Minerals Society Source Clays: Powder X-ray diffraction analyses. *Clays Clay Miner.* **2001**, *49*, 398−409.
(26) Jaynes, W. F.; Bigham, J. M. Multiple cation-exchange capacity measurements on standard clays using a commercial mechanical extractor. *Clays Clay Miner.* **1986**, *34*, 93−98.
(27) Jaynes, W. F.; Bigham, J. M. Charge reduction, octahedral charge, and lithium retention in heated, Li-saturated smectites. *Clays Clay Miner.* **1987**, *35*, 440−448.
(28) Madejova, J.; Komadel, P. Baseline studies of The Clay Minerals Society Source Clays: Infrared methods. *Clays Clay Miner.* **2001**, *49*, 410−432.
(29) Mermut, A. R.; Cano, A. F. Baseline studies of The Clay Minerals Society Source Clays: Chemical analyses of major elements. *Clays Clay Miner.* **2001**, *49*, 381−386.
(30) Mermut, A. R.; Lagaly, G. Baseline studies of The Clay Minerals Society Source Clays: Layer-charge determination and characteristics of those minerals containing 2:1 layers. *Clays Clay Miner.* **2001**, *49*, 393−397.
(31) *Data Handbook for Clay Materials and Other Non-Metallic Minerals*; Olphen, H. v., Fripiat, J. J., Eds.; Pergamon Press: New York, 1979.
(32) Loring, J. S.; Thompson, C. J.; Wang, Z. M.; Joly, A. G.; Sklarew, D. S.; Schaef, H. T.; Ilton, E. S.; Rosso, K. M.; Felmy, A. R. *In situ* infrared spectroscopic study of forsterite carbonation in wet supercritical CO_2. *Environ. Sci. Technol.* **2011**, *45*, 6204−6210.
(33) Thompson, C. J.; Loring, J. S.; Rosso, K. M.; Wang, Z. M. Comparative reactivity study of forsterite and antigorite in wet supercritical CO_2 by in situ infrared spectroscopy. *Int. J. Greenhouse Gas Control* **2013**, *18*, 246−255.
(34) Schneider, M. S.; Grunwaldt, J. D.; Burgi, T.; Baiker, A. High pressure view-cell for simultaneous in situ infrared spectroscopy and phase behavior monitoring of multiphase chemical reactions. *Rev. Sci. Instrum.* **2003**, *74*, 4121−4128.
(35) Thompson, C. J.; Martin, P. F.; Chen, J.; Schaef, H. T.; Rosso, K. M.; Felmy, A. R.; Loring, J. S. Automated high-pressure titration system with *in situ* infrared spectroscopic detection. *Rev. Sci. Instrum.* **2014**, in press.
(36) Sato, T.; Watanabe, T.; Otsuka, R. Effects of layer charge, charge location, and energy change on expansion properties of dioctahedral smectites. *Clays Clay Miner.* **1992**, *40*, 103−113.
(37) Wang, Z. M.; Felmy, A. R.; Thompson, C. J.; Loring, J. S.; Joly, A. G.; Rosso, K. M.; Schaef, H. T.; Dixon, D. A. Near-infrared spectroscopic investigation of water in supercritical CO_2 and the effect of $CaCl_2$. *Fluid Phase Equilib.* **2013**, *338*, 155−163.
(38) Spycher, N.; Pruess, K.; Ennis-King, J. CO_2-H_2O mixtures in the geological sequestration of CO_2. I. Assessment and calculation of mutual solubilities from 12 to 100 °C and up to 600 bar. *Geochim. Cosmochim. Acta* **2003**, *67*, 3015−3031.
(39) Hur, T.-B.; Baltrus, J. P.; Howard, B. H.; Harbert, W. P.; Romanov, V. N. Carbonate formation in Wyoming montmorillonite under high pressure carbon dioxide. *Int. J. Greenhouse Gas Control* **2013**, *13*, 149−155.
(40) Romanov, V. N. Evidence of irreversible CO_2 intercalation in montmorillonite. *Int. J. Greenhouse Gas Control* **2013**, *14*, 220−226.
(41) Anderson, R. L.; Ratcliffe, I.; Greenwell, H. C.; Williams, P. A.; Cliffe, S.; Coveney, P. V. Clay swelling - A challenge in the oilfield. *Earth-Sci. Rev.* **2010**, *98*, 201−216.
(42) Landsbaum, E. M.; Dodds, W. S.; Stutzman, L. F. Humidity of compressed air. *Ind. Eng. Chem.* **1955**, *47*, 101−103.
(43) de Siqueira, A. V.; Lobban, C.; Skipper, N. T.; Williams, G. D.; Soper, A. K.; Done, R.; Dreyer, J. W.; Humphreys, R. J.; Bones, J. A. R. The structure of pore fluids in swelling clays at elevated pressures and temperatures. *J. Phys.: Condens. Matter* **1999**, *11*, 9179−9188.
(44) Skipper, N. T.; Williams, G. D.; de Siqueira, A. V. C.; Lobban, C.; Soper, A. K. Time-of-flight neutron diffraction studies of clay-fluid interactions under basin conditions. *Clay Miner.* **2000**, *35*, 283−290.
(45) de Siqueira, A. V. C.; Skipper, N. T.; Coveney, P. V.; Boek, E. S. Computer simulation evidence for enthalpy driven dehydration of smectite clays at elevated pressures and temperatures. *Mol. Phys.* **1997**, *92*, 1−6.

(46) Ransom, B.; Helgeson, H. C. A chemical and thermodynamic model of aluminous dioctahedral 2:1 layer clay minerals in diagenetic processes; regular solution representation of interlayer dehydration in smectite. *Am. J. Sci.* **1994**, *294*, 449−484.
(47) Madsen, F. T. Surface-area measurements of clay-minerals by glycerol sorption on a thermobalance. *Thermochim. Acta* **1977**, *21*, 89−93.
(48) Schaef, H. T.; Glezakou, V. A.; Owen, A. T.; Ramprasad, S.; Martin, P. F.; McGrail, B. P. Surface condensation of CO_2 onto kaolinite. *Environ. Sci. Technol. Lett.* **2013**, *1*, 142−145.
(49) Ferrage, E.; Lanson, B.; Michot, L. J.; Robert, J. L. Hydration properties and interlayer organization of water and ions in synthetic Na-smectite with tetrahedral layer charge Part 1. Results from X-ray diffraction profile modeling. *J. Phys. Chem. C* **2010**, *114*, 4515−4526.
(50) Tunega, D.; Gerzabek, M. H.; Lischka, H. Ab initio molecular dynamics study of a monomolecular water layer on octahedral and tetrahedral kaolinite surfaces. *J. Phys. Chem. B* **2004**, *108*, 5930−5936.
(51) Hatch, C. D.; Wiese, J. S.; Crane, C. C.; Harris, K. J.; Kloss, H. G.; Baltrusaitis, J. Water adsorption on clay minerals as a function of relative humidity: application of BET and Freundlich adsorption models. *Langmuir* **2012**, *28*, 1790−1803.
(52) Cases, J. M.; Berend, I.; Francois, M.; Uriot, J. P.; Michot, L. J.; Thomas, F. Mechanism of adsorption and desorption of water vapor by homoionic montmorillonite 3. The Mg^{2+}, Ca^{2+}, Sr^{2+} and Ba^{2+} exchanged forms. *Clays Clay Miner.* **1997**, *45*, 8−22.